Adsorption of rare earth elements by unmodified natural magnetite from Phalaborwa, South Africa: Equilibrium isotherms, kinetic models and thermodynamic studies

Kitondo Mwelwa[1,2], Imasiku Nyambe[3], Hlanganani Tutu[1], Luke Chimuka[1,*]

[1]*Molecular Sciences Institute, School of Chemistry, University of the Witwatersrand, Johannesburg, South Africa.*
[2]*School of Mathematics and Natural Sciences, Copperbelt University, Kitwe, Zambia.*
[3]*Geology Department, School of Mines, University of Zambia, Lusaka, Zambia.*

ABSTRACT

Adsorption studies of $REEs^{3+}$ by unmodified natural magnetite was investigated. Characterisation of sorbent material was conducted by XRD, XRF and leaching techniques. Experiments to determine the influence of some determinant factors (adsorbent mass, agitation time, pH, initial concentration and temperature) on adsorption processes yielded necessary data for plotting graphs leading to equilibrium isotherms, kinetic models and thermodynamic studies. Unmodified natural magnetite contained principally Fe_3O_4 (~88%) and a few impurities (~12%), but no REEs. Optimum recovery capacities were established at 90 minutes agitation time, pH 4.5, initial concentration 1.7 mg L^{-1} and 150 mg adsorbent mass. The adsorption process fitted better the Langmuir isotherm, was described by the PSO kinetic model and was thermodynamically spontaneous. With reference to standard limits of adsorption energy (Es, [8 – 16 kJ mol^{-1}]) and standard enthalpy change (ΔH^o < 40 kJ mol^{-1}), the adsorption mechanism was ion exchange in nature. However, activation energy was split between physisorption (Ea < 40 kJ mol^{-1}) and chemisorption (Ea > 80 kJ mol^{-1}) processes.

KEYWORDS

Adsorption, Rare earth elements, unmodified natural magnetite, isotherms, Phalaborwa

Received 3 April 2024, revised 5 November 2024, accepted 26 November 2024

INTRODUCTION

Within the Periodic Table, the series of Lanthanide elements, from lanthanum (La) to lutetium (Lu), together with scandium (Sc) and yttrium (Y), form a collection of elements known as rare earth elements (REEs). They are differentiated as light rare earth elements (LREEs) comprised of La, Ce (cerium), Pr (praseodymium), Nd (neodymium), Pm (promethium), and as heavy rare earth elements (HREEs) consisting of Sm (samarium), Eu (europium), Gd (gadolinium), Tb (terbium), Dy (dysprosium), Ho (holmium), Er (erbium), Tm (thulium), Yb (ytterbium), Lu and Y [1-4].

Rare earth elements are relatively abundant in the earth crust, and China has enjoyed, for a long time now, the status of world repository of REEs reserves [2,5]. However, the unfolding of new developments has shown that new discoveries of REEs deposits have extended their distribution to various locations in all continents [2,4,6]. Regardless of these discoveries, fundamental questions, as to whether most of these REEs primary resources (ores and minerals) are practically and economically minable for industrial production, have been raised[7]. To this regard, cautionary advice has been conveyed to channel REEs mining investments into ventures supported by solid scientific data, sound innovative approaches and suitable environmental considerations[5]. Attention has also been attracted to apatite concentrate from igneous phosphate [4,8] and to high-tech industry scraps or "urban mining" [5,9] as potent REEs secondary resources.

The multi-applicability of REEs unique magnetic, catalytic, optical, electrical and metallurgical properties have proved crucial to high-tech (e.g. smart devices), clean energy (e.g. wind turbine generators, electric vehicles…) and futuristic industries (e.g. medical, aerospace…)[1,7]. Owing to these fields of application in modern economies, the rise in REEs consumption coupled with the risk of supply disruption have greatly influenced the increase in their market value[5]. This situation has been exacerbated by the fact that China is, by far (>95%), the largest producer and supplier of REES in the world[5,10]. The call to reduce the gap between the demand for REEs and the supply of REEs, and possibly meet future demand, can never be more heedful[3].

In recent years, research about the recovery of $REEs^{3+}$ in solutions has increased in numbers[11-14], and various methods have been studied among which adsorption has attracted particular attention as a better way to recover REEs ions because of its simplicity, high efficiency and cost effectiveness[7,11,15,16]. A review by Anastopoulos, Bhatnagar and Lima (2016) presented different adsorbent materials including raw and modified organic compounds as well as natural, modified and synthetic inorganic materials for single or multi-REEs ions removal from solutions. Batch and column adsorption techniques have been commonly used in this endeavour[14,17].

Iron oxy-hydroxide materials, e.g. hematite (Fe_2O_3), goethite (FeOOH) and magnetite (Fe_3O_4), are common in the environment, magnetic, semi-conducting, easy to prepare in the lab and have large surface area. Functional groups at their surface exert some attractive influence on particles in their immediate surroundings[18]. They can participate in redox reactions by transferring electrons to higher valence cation species at the solid-liquid interface. The use of iron oxy-hydroxide materials as adsorbent, in their natural or modified forms, for the removal of trace elements, the recovery of precious group metals (PGM) and REEs has been reported[7,19]. Findings by Alorro *et al.* (2010) relative to the adsorption recovery capabilities of natural magnetite for gold were remarkable and appealing. However, the use of unmodified natural magnetite for the recovery of REEs does not appear on the comprehensive list of adsorbent materials previously employed[1]. Besides, the same list has been reproduced in recent publication[16], implying the status quo remains.

This study focuses on adsorption processes between $REEs^{3+}$ in solution (adsorptive) and unmodified natural magnetite (adsorbent) employing a batch method with the aim of evaluating the adsorbent potential to take up $REEs^{3+}$. In this regard, equilibrium isotherms, kinetics models and thermodynamics studies were investigated.

*To whom correspondence should be addressed
Email: Luke.Chimuka@wits.ac.za

ISSN 1996-840X Online / South African Chemical Institute / http://saci.co.za/journal

https://doi.org/10.17159/0379-4350/2024/v78a38

MATERIALS AND METHODS

Characterisation of magnetite and preparation of $REEs^{3+}$ solutions

Natural magnetite, collected from mine waste piles in Phalaborwa, South Africa, was sieved to obtain reduced size particles (<50 µm diameter) which were used, without any modification, (1) for characterisation in terms of mineralogical composition by XRD analysis (Bruker D2 Phaser powder diffractometer Co $K_{\alpha 1}$, Germany) and elemental content by XRF technique (Axios Max, Analytica, the Netherlands), and (2) for multi-$REEs^{3+}$ batch adsorption experiments. To assess the possible release of $REEs^{3+}$ into the adsorption fluid, magnetite was subjected to leaching with HNO_3 solutions of similar concentrations to $REEs^{3+}$ adsorptive solutions employed in batch adsorption experiments.

Analytical grade multi-element $REEs^{3+}$ standards solution (1000 mg L^{-1} in HNO_3) from Sigma Aldrich, South Africa, was used to prepare 100 mg L^{-1} stock solution in a 50 mL graduated polyethylene centrifuge tube. This solution was used for further dilutions to desired concentrations of fresh working solutions as per adsorption experiments dictate. Selected solid salts ($CaCl_2$, $MgSO_4$, $CuCl_2$, $ZnSO_4.4H_2O$, $MnSO_4.4H_2O$, $NiSO_4$, $CoSO_4.7H_2O$, $Pb(NO_3)_2$) were also used to prepare single element stock solutions (50 mL, 100 mg L^{-1}) of competing ions. Appropriate amounts of these stock solutions were then mixed to obtain multi-element working solutions of competing ions. Deionized water (DI), 18 Ω cm^{-1}, drawn from a Milli-Q system (Millipore Corp., Bedford, MA, USA), was used in the preparation and dilution processes.

Adsorption experiments

A batch method was used to carry out adsorption experiments. Triplicates of closed polyethylene centrifuge tubes, containing equal amounts of natural magnetite (mg) and a constant volume of multi-$REEs^{3+}$ solution (15 mL) were shaken at 150 rpm and room temperature (25°C). In order to allow for adsorption isotherms, kinetics models and thermodynamic studies, experiments leading to the attainment of equilibria were conducted under varying conditions of adsorbent mass, pH conditions, agitation time, initial concentration and temperature, as shown in Table 1. Experiments involving competing ions (a factor not included in Table 1) were also carried out with all other factors set at optimum conditions except for initial concentration. At the end of agitation, adsorptive-adsorbent mixtures were centrifuged (5 min, 3000 rpm), the supernatants passed through syringe filters (0.22 µm) and analysed by ICP-OES (Spectro Genesis, Germany; operated with the Smart Analyser Vision Software 6.01.0943). A good reproducibility was obtained, and standard deviations were always less than 5% of mean values.

Along the progression of adsorption experiments towards the attainment of equilibria, measurements of $REEs^{3+}$ concentration remaining in solution at time t (C_t) or at equilibrium (C_{eql}) versus the corresponding amount of $REEs^{3+}$ adsorbed on to natural magnetite at time t (q_t) or at equilibrium (q_{eql}) constituted, directly or indirectly, the foundation for all plots necessary for this study. To this effect, experimental data were fed into different equations relative to equilibrium (Equation 1), kinetics (Equation 2 and 3) and thermodynamic (Equation 4) adsorption studies. Some of these equations are described below[20-23]:

$$q_{eql} = (C_i - C_{eql})\ V/m \qquad \text{isotherm model} \qquad \text{Equation 1}$$

where q_{eql} is the amount of adsorptive taken up by the adsorbent at equilibrium (mg g^{-1}), Ci is the initial concentration of adsorptive in solution (mg L^{-1}), C_f is the final concentration of adsorptive in solution (mg L^{-1}), V is the volume of solution (L) and m is the mass of adsorbent (g).

$$\ln (q_{eql} - q_t) = \ln q_{eql} - k_1 t \qquad \text{pseudo-first-order (PFO) kinetic model} \qquad \text{Equation 2}$$

$$t/q_t = 1/(k_2 q_{eql}^2) + (1/q_{eql})t \qquad \text{pseudo-second-order (PSO) kinetic model} \qquad \text{Equation 3}$$

where q_{eql} is the amount of adsorptive taken up by the adsorbent at equilibrium (mg g^{-1}), q_t is the amount of adsorptive taken up by the adsorbent at time t (mg g^{-1}), k_1 is the PFO kinetic rate constant (min^{-1}), k_2 is the PSO kinetics rate constant (g (mg $min)^{-1}$) and t is the agitation time (min).

$$K_d = q_{eql}/C_{eql} \qquad \text{apparent equilibrium constant} \qquad \text{Equation 4}$$

where K_d is the apparent equilibrium constant, q_{eql} is the amount of adsorptive taken up by the adsorbent at equilibrium (mg g^{-1}), C_{eql} is the equilibrium concentration of the adsorptive solution (mg L^{-1}).

Mathematical treatment of plots line equations yielded parameters necessary for interpreting REEs adsorption processes: (1) equilibrium data, obtained for different initial concentrations, were evaluated using the Langmuir, Freundlich and Dubinin-Radushkevich isotherm models; (2) kinetics data, obtained at various intervals of time, were assessed using Lagergren pseudo-first-order (PFO) and Ho & McKay pseudo-second-order (PSO) kinetics models; (3) thermodynamic data, obtained at different temperatures, were used to calculate different parameters associated with heats of adsorption.

RESULTS AND DISCUSSION

Characterisation of magnetite

Powder X-ray diffraction technique detected a pure crystalline phase of iron oxide ($Fe^{II}2Fe^{III}O_4$), with no evidence of other mineral phases in the sample (Figure 1). X-ray fluorescence analysis for major elements was also typical of natural magnetite as it contained essentially Fe_3O_4 (88.05%). Some impurities of SiO_2 (4.78%), MgO (3.09%), TiO_2 (1.76%), CaO (1.26%) and other metal oxides (<1%) were also found in the sample. Leaching of unmodified natural magnetite with HNO_3 showed undetectable amounts of $REEs^{3+}$ in leachates. It was noted that the percentage purity of natural magnetite from Iron County, Utah, USA, used in the recovery of gold had a comparatively lower percent purity (82.2%)[19].

Table 1: Factors in batch adsorption experiments of $REEs^{3+}$ on to unmodified natural magnetite

Factor	Variable conditions	Adsorbent (mg)	Initial pH	Contact time (min)	Initial concentration (mg L^{-1})	Temperature
Adsorbent (mg)	50, 100, 150, 200, 300, 500	Varied	2.2 unadjusted	300	1.0	25°C
pH	2.5, 4.5, 6, 7, 9.5	Optimum	Varied	300	1.0	25°C
Contact time (min)	30, 60, 90, 135, 180, 240	Optimum	Optimum	Varied	1.0	25°C
Initial concentration (mg L^{-1})	0.1, 0.5, 1.0, 1.5, 2.0, 2.5	Optimum	Optimum	Optimum	Varied	25°C
Temperature (°C)	25, 35	Optimum	Optimum	Optimum	mixed	Varied

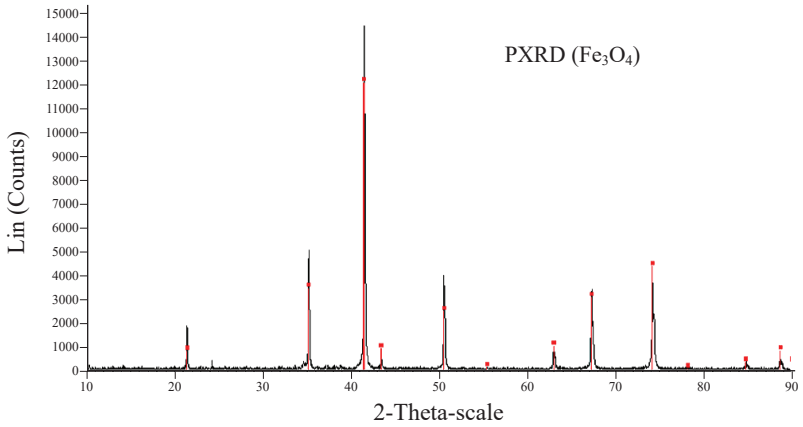

Figure 1: Powder X-ray diffraction data collected on unmodified natural magnetite. Scale and legend: horizontal axis = 2-Theta-scale (10 to 90) and vertical axis = Lin (Counts) (0 to 15,000)

Optimization of adsorption factors

Different factors influencing adsorption processes of $REEs^{3+}$ by unmodified natural magnetite were carefully assessed following the protocol given in Table 1 above. Determining the optimum value of a factor in the preceding experiment had a bearing on the results of all subsequent optimization experiments. A replicate of Table 1 could be redrawn to show, actual values of factors in place of the generic term "optimum". Instead, a narrative about results and tendencies shown by optimization experiments is presented below. Even though all $REEs^{3+}$ are presented in different Figures below, some of them are depicted by solid lines (Ce, Eu, La, Nd, Dy and Y) mainly because they have been commonly used in $REEs^{3+}$ leaching and adsorption studies with a variety of adsorbents, but also because they are critical in emerging green energy technologies [1,5]. They were, therefore, selected to show the influence of different factors on adsorption processes in this study.

Effects of adsorbent mass

Figure 2 displays lines curvatures conveying a similar response behaviour of $REEs^{3+}$ to adsorption processes. These curved lines were plotted using data obtained from simultaneous shaking of six test tubes containing the same volume and initial concentration of $REEs^{3+}$ but increasing masses of unmodified natural magnetite (Table 1). At the end of the agitation period, the amount of $REEs^{3+}$ adsorbed on to 50 mg, 100 mg and 150 mg natural magnetite was successively higher. On the contrary, the amount of $REEs^{3+}$ adsorbed on to 200 mg, 300 mg and 500 mg of natural magnetite was successively lower. In both instances, higher adsorbent masses availed more adsorption sites to the same amount of adsorptive. However, in the first instance, 50 mg, 100 mg and 150 mg adsorbent drew adsorptive from solution, in proportion to the available number of adsorption sites. Even though adsorbent masses were increased, the number of adsorption sites were still lower than the amount of adsorptive in solution but tending towards matching. It was observed that the amount of $REEs^{3+}$ adsorbed by natural magnetite was high for 50 mg, higher for 100 mg and highest (at the pick of the curve) for 150 mg. This suggested that the number of adsorption sites on 150 mg natural magnetite almost matched the amount of $REEs^{3+}$ in solution. In the second instance, 200, 300 and 500 mg removed "all" adsorptive from solution, implying that these quantities availed more adsorption sites as opposed to the amount of adsorptive in solution. Therefore, after reaching equilibrium, there were more adsorption sites remaining unoccupied. It was observed that, for theses higher masses, adsorption capacities got successively lower and drifted away from the optimum point, i.e. the point at which the maximum number of adsorptive is removed from solution for a full occupation of adsorption sites on the adsorbent.

Taking it that $REEs^{3+}$ in solution were competing among themselves for fewer adsorption sites, it was observed from Figure 2 that at 50 mg

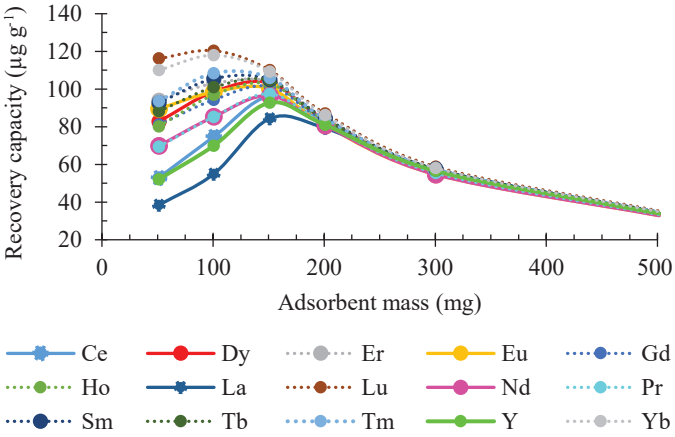

Figure 2: Effect of adsorbent dosage changes on adsorption capacity

adsorbent there was a wide gap (of ~80 µg g^{-1}) between the highest adsorption capacities (Yb > Lu > Tm) and the lowest adsorption capacities (La < Y < Ce). This gap grew smaller at higher adsorbent masses (70, 40, 10 µg g^{-1} at 100, 150 and 200 mg). This observation means that unmodified natural magnetite is selective, i.e. it does not have the same affinity for all $REEs^{3+}$ which are consequently not taken up at the same rate. Those with higher rate (Yb, Lu, Tm) adsorbed faster and reached maximum capacity (120.4, 117.9 and 108.4 µg g^{-1} respectively) at smaller adsorbent mass (100 g), while those with lower rate (La, Y, Ce) reached maximum capacity at larger adsorbent mass (150 mg). For most $REEs^{3+}$, the recovery capacity was highest for 150 mg adsorbent. It ranged from 84.3 to 109.3 µg g^{-1} (average 99.0 µg g^{-1}). With reference to five out of the six $REEs^{3+}$ depicted by solid lines in Figure 2, the adsorbent mass of 150 mg unmodified natural magnetite was considered optimum for use in the next step.

Effects of contact time

Figure 3 shows that adsorption capacity increased by a tremendous amount within the first 30 minutes with the lowest being ~60 µg g^{-1} for La and highest being ~90 µg g^{-1} for Yb. Within the next 30 minutes the increase was moderate (~10 µg g^{-1}) to negligible (~5 µg g^{-1}) for Yb and La respectively. By 90 minutes most $REEs^{3+}$ had been removed from solution. Most $REEs^{3+}$ were rapidly adsorbed within the shortest agitation period where virgin adsorbent, with more readily available adsorption sites, permitted near maximum $REEs^{3+}$ uptake. It was observed, here too, that unmodified natural magnetite showed similar selectivity for $REEs^{3+}$ as for adsorbent dosage but increasing agitation time did not affect the gap between $REEs^{3+}$ with higher and lower adsorption capacities. Average adsorption capacities were 81.5, 88.4, 89.2, 89.9, 94.8 and 95.0 µg g^{-1}-for 30, 60, 90, 135, 180 and 240 minutes

of continuous agitations. Working with average values, 90 minutes was considered optimum time after which agitation became counter-productive.

Figure 4 shows descending curves of reducing adsorption capacities with increasing agitation time. It was obtained by factoring time ratios in the recovery equation in order to bring down recovery capacities to the same agitation time (here, 30 minutes). A different perspective of the recovery capacity was obtained in support of the fact that the intensity of $REEs^{3+}$ adsorption on to unmodified natural magnetite was quickly diminishing with time. This is shown by the assigning of 81.5, 44.2, 29.7, 19.9, 15.8 and 11.8 μg g^{-1} to 30, 60, 90, 135, 180 and 240 minutes of continuous agitations.

A separate sequential (relay) batch recovery experiment was performed to assess the effect of agitation period on the recovery efficiency of $REEs^{3+}$ by unmodified natural magnetite. Test tubes containing adsorbent-adsorptive mixtures were shaken for 30 minutes. The supernatant was transferred immediately into centrifuge tubes containing the same mass of unused (virgin) natural magnetite. The new mixtures were also agitated for 30 minutes. Results showed that adsorption efficiency was over 50% within the first 30 minutes of agitation, and increased to almost full capacity within the second 30 minutes of agitation with new adsorbent. Therefore, at 60 minutes of total agitation, all $REEs^{3+}$ left from the first 30 minutes agitation were taken up by unmodified natural magnetite during the second 30 minutes agitation. The recovery efficiency of $REEs^{3+}$ was 99.8% at 60 minutes, distributed as 76.5% in the first 30 minutes and 23.3% in the second 30 minutes (Figure 5). This efficiency could not be achieved by 240 minutes of continuous agitation (89.1%). This method is commonly used in metal floatation recovery and was evaluated by Santos Yabe and de Oliveira (2003) for the removal of toxic metals from industrial effluents by sequential adsorbent treatment [24].

Effects of pH

Quite similar $REEs^{3+}$ adsorption behaviours are depicted, in different pH conditions, by curved lines shown in Figure 6. Adsorption capacity was high in strong acidic conditions (pH 2.5), increased in moderate acidic (pH 4.5) and weak a little in mild acidic (pH 6.0) conditions; it reduced a little further in neutral and mild alkaline conditions (pH 7.0 and 8.0) before dropping abruptly to insignificant levels in medium alkaline conditions (pH 9.5). The plausible explanation to this observation is that hydroxide ions (OH^-), used for adjusting adsorptive carrying solution pH to desired higher values, had reacted with $REEs^{3+}$ cations to form insoluble REE hydroxides (REEOHs)[7], thereby reducing the amounts of free $REEs^{3+}$ available for adsorption. A similar observation was made by Khawassek *et al.* (2015) in the recovery of $REEs^{3+}$ by precipitation using NaOH and NH_4OH solutions[13]. Using the theory of hard and soft acid and base theory, Elsaidi *et al.* (2018) attributed this behaviour of $REEs^{3+}$ to their hard acid properties (cations with higher oxidation state and low polarizability) which give them higher affinity for hard bases (high electronegativity and highest occupied molecular orbitals) such as OH^-[7].

It was observed that $REEs^{3+}$ with lower recovery capacities in acidic medium (e.g. La, Ce and Y) showed higher recovery capacities in neutral and mild alkaline conditions. This is noticeable at pH 7 and 8, assumingly, because these $REEs^{3+}$ had lower affinity for OH^- and, as such, precipitated less during incremental adjustments of pH, and were consequently more available for adsorption by unmodified natural magnetite. Conversely, $REEs^{3+}$ with higher recovery capacities in acidic medium (e.g. Tb, Eu and Dy) showed lower recovery capacities in neutral and mild alkaline conditions. This is also noticeable at pH 7 and 8, assumingly, because these $REEs^{3+}$ had higher affinity for OH^- and, as such, precipitated more during incremental adjustments of pH, and were consequently less

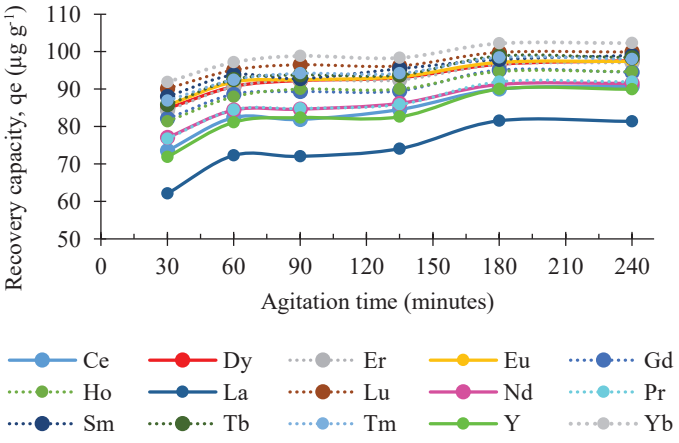

Figure 3: Effect of agitation time changes on adsorption capacity

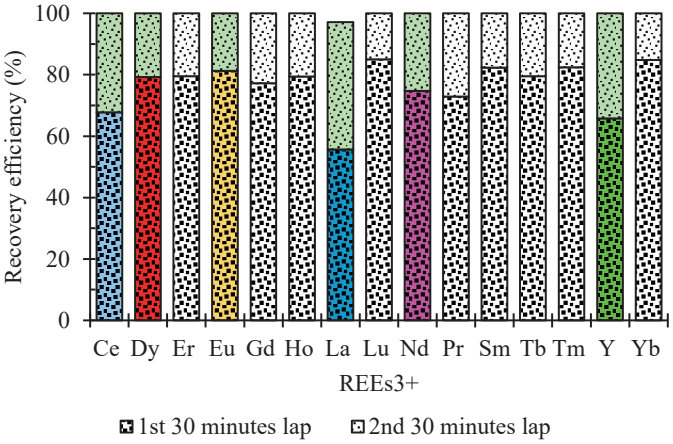

Figure 5: Effect of sequential (relay) recovery on adsorption capacity

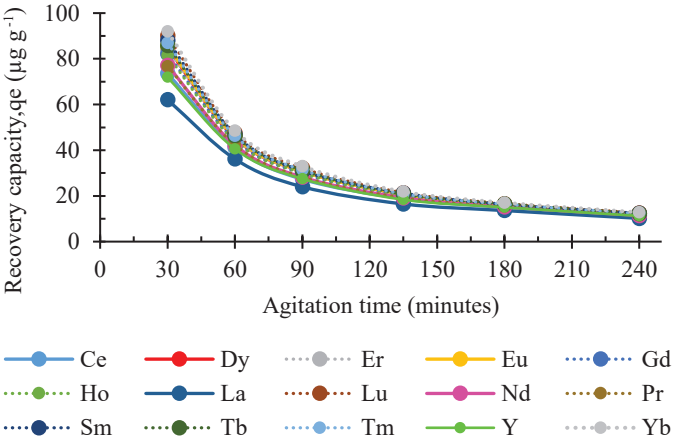

Figure 4: Effect of agitation time on the intensity of adsorption process

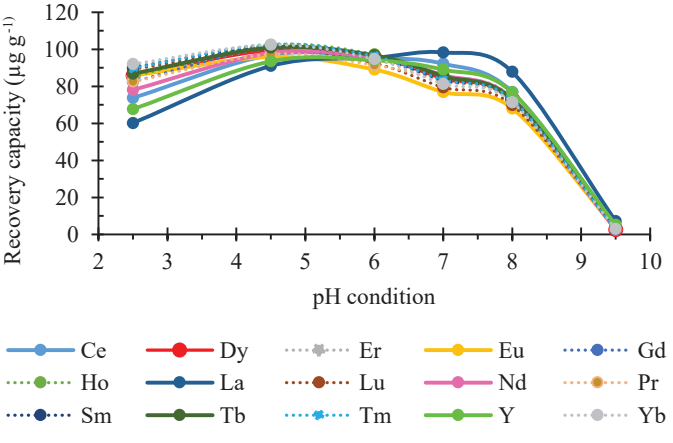

Figure 6: Effect of pH conditions on adsorption capacity

available for adsorption by unmodified natural magnetite. These similar but opposite precipitation responses of $REEs^{3+}$ (e.g. La, Ce, Y versus Yb, Eu and Dy) to OH^- additions were observed on both sides of pH 6 which was taken to be the changeover point for adsorbent selectivity. However, the point of zero charge was not investigated in detail under the study of the influence of pH on adsorption. At pH 9.5 the percentage precipitation of all $REEs^{3+}$ was ~100%.

Analytical measurements of adsorptive carrying solution, prior to mixing with natural magnetite, revealed that $REEs^{3+}$ followed the same pattern. Cerium (Ce) concentration in the initial solution (pH 2.3) was 1.087 mg L^{-1} before pH incremental adjustment. Cerium concentration changed slightly to 1.077 mg L^{-1}, 1.042 mg L^{-1}, 0.995 mg L^{-1}, 0.922 mg L^{-1} at pH 2.5, 4.5, 6 and 7, but changed moderately to 0.77 mg L^{-1} and significantly to 0.046 mg L^{-1} at pH 8 and 9.5 respectively. Ytterbium (Yb) concentration in the initial solution (pH 2.3) was 1.089 mg L^{-1} before pH incremental adjustment. Ytterbium concentration changed slightly to 1.082 mg L^{-1}, 1.046 mg L^{-1}, 0.954 mg L^{-1}, 0.813 mg L^{-1} at pH 2.5, 4.5, 6 and 7, but changed moderately to 0.714 mg L^{-1} and significantly to 0.029 mg L^{-1} at pH 8 and 9.5 respectively. It was clear that free $REEs^{3+}$ had reacted with OH^- and that the extent of this reaction was noticeable in neutral and mild alkaline condition (pH 8) and severe thereafter (pH 9.5) leaving in solution an insignificant amount of free $REEs^{3+}$ available for adsorption. The small amount of $REEs^{3+}$ left in the adsorptive carrying solution at pH 8 was all taken up in a quick exhaustion by the adsorbent; this amount of $REEs^{3+}$ could only occupy a very small number of adsorption sites on unmodified natural magnetite, changing completely the recovery scenario. For most $REEs^{3+}$, the recovery capacity was highest at pH 4.5 (Figure 6), ranging from 91.0 (La) to 102.5 μg g^{-1} (Yb) with an average of 98.9 μg g^{-1}. Therefore, pH 4.5 was the adopted candidate for the next step of reactions.

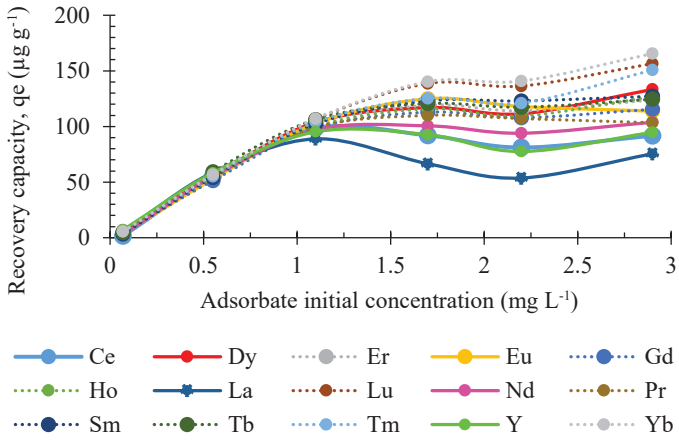

Figure 7: effect of initial concentration changes on adsorption capacity

Effects of initial concentration

Figure 7 shows a substantial and progressive increase in adsorption capacities for lower initial concentrations followed by a minimal decrease in adsorption capacities for higher initial concentrations. Increasing initial concentrations provided increasing amounts of $REEs^{3+}$ in solution for a constant number of adsorption sites on unmodified natural magnetite. The first two or three segments of the ascending plot line signify that there were more adsorption sites on unmodified natural magnetite to cater for all $REEs^{3+}$ in solution, and that adsorption continued without any competition among $REEs^{3+}$. Because of excessive adsorption sites on the adsorbent, selectivity did not apply and adsorption capacities were similar for all $REEs^{3+}$. Competition among $REEs^{3+}$ started when the amount of $REEs^{3+}$ became higher than the total number of adsorption sites. This is shown by the separation of lines indicating that the adsorbent started adsorbing $REEs^{3+}$ selectively. Considering the adsorption pattern followed by $REEs^{3+}$, the highest adsorption capacity was found to be ~ 1.2 mg L^{-1} for some $REEs^{3+}$ (e.g. La and Ce) and ~ 1.7 mg L^{-1} for most other $REEs^{3+}$ (e.g. Er, Nd, Yb, Lu). The calculated average adsorption capacity was 113 μg g^{-1} and correlated with 1.7 mg L^{-1} $REEs^{3+}$ initial concentration.

Effect of competing ions

The recovery efficiency obtained from the agitation (150 rpm, 180 minutes) $REES^{3+}$ solution (15 mL, pH 4.5 and ~0.5 mg L^{-1}), and a second solution (15 mL, pH 4.5) containing a mixture of $REES^{3+}$ (~0.5 mg L^{-1}) and competing ions of higher and varying concentrations (1.0 – 2.5 mg L^{-1}), with unmodified natural magnetite (150 mg) in 50 mL centrifuge tubes are presented in Figure 8 below. REEs average recovery efficiency was ~99.0% in $REEs^{3+}$ solution (Figure 8a), but it dropped only to ~95.0% in the mixed solution (Figure 8b)

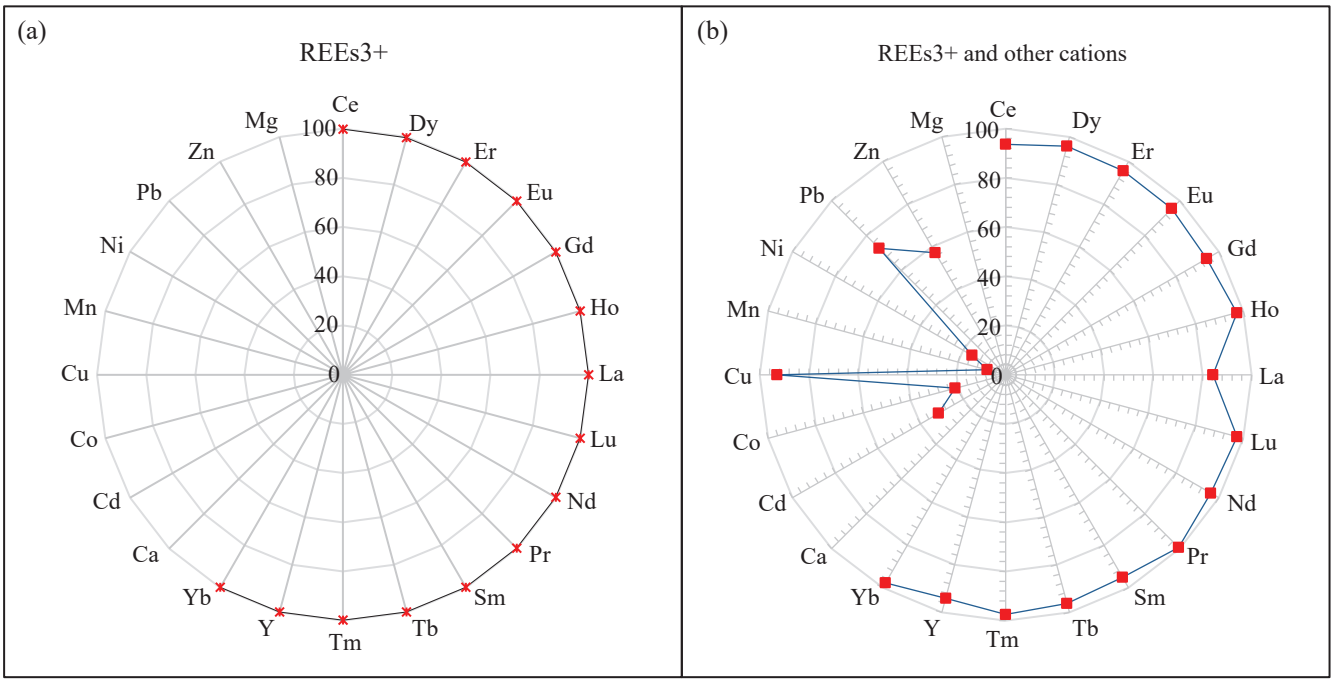

Figure 8: Effect of competing ions on adsorption capacity

where unmodified natural magnetite selectivity was equally higher for Cu^{2+}, moderate for Pb^{2+} and Zn^{2+}, and much lower for Cd^{2+}, Co^{2+}, Mn^{2+} and Ni^{2+}. Figure 8b shows that the recovery efficiency of $REEs^{3+}$ was minimally affected by the presence of other competing ions in solution. This behaviour raised some speculative predictions as to what the influence of higher concentrations of competing ions on the recovery of REEs would be in the natural environment (e.g. water retain dam, effluent) where the gap in concentrations between $REEs^{3+}$ and most competing ions (usually trace elements) is normally huge. With reference to Elsaidi *et al.* (2018), $REEs^{3+}$ are hard Lewis acids which, in the natural environment, enjoy competitive advantage in their interactions with hard Lewis bases (e.g. oxy-hydroxides at mineral surfaces) than soft Lewis acid such as trace element cations[7].

Kinetic studies

Experimental data from the effect of varying agitation time was used in the linear expression of the Lagergren pseudo first-order (PFO) and the Ho & McKay pseudo second-order (PSO) kinetic model rate equations. PFO kinetic model plots (ln(qe–qt) vs t) produced negative sloping lines with low correlation coefficients (R^2 = 0.796). Adsorption capacities calculations ensuing from these line equations ($q_{e,calc}$) were quite different from experimental adsorption capacities ($q_{e,exp}$). Conversely, PSO kinetics model plots (t/q_t vs t) produced positive sloping lines with very high correlation coefficient (R^2 = 0.999). Adsorption capacities calculated from PSO kinetic model plot line equations ($q_{e,calc}$) were lower but consistently close to values of experimental adsorption capacities ($q_{e,exp}$). By comparing results of these two kinetic models, it was found that PSO had better correlation coefficients and yielded acceptable values of calculated adsorption capacities than corresponding parameters of PFO. Therefore, PSO kinetic model was a better candidate for explaining kinetic adsorption processes of $REEs^{3+}$ by unmodified natural magnetite.

Following this deliberation, the rate constant of PSO kinetic model (k_2) was adequate for calculating the activation energy (Ea) using the Arrhenius plot ($\ln k_2$ vs 1/T). Positive activation energies were calculated from the line equations, indicating that $REEs^{3+}$ required some energy to surmount the energy barrier for adsorption to occur. In conformity to the Arrhenius equation, the rate of adsorption decreased when temperature was increased (Table 2).

Comparing the Ea obtained here with demarcation limits set in literature (Inglezakis and Zorpas, 2012), as shown in Table 3, it could be said that adsorption of some $REEs^{3+}$ (Dy, Er, Eu, Ho, Lu, Tb and Yb) onto unmodified natural magnetite belonged to the physisorption type of mechanism (Ea < 40 kJ mol^{-1}) whereas other $REEs^{3+}$ (Ce, Gd, La, Nd, Pr, Sm and Y) onto unmodified natural magnetite was of the Chemisorption type of mechanism (Ea > 40 kJ mol^{-1}). Most of those classified as undergoing physisorption could be further clustered as undergoing ion exchange (40 kJ mol^{-1} > Ea > 24 kJ mol^{-1}). Based on Ea values obtained, adsorption processes could not be said to be entirely physisorption or chemisorption in nature.

Isotherms studies

Langmuir isotherm

Both, curvilinear (q_t versus C_t) and linear (q_{eq}/C_{ads} versus lines C_{eq}) plots of the Langmuir isotherm were obtained from experimental data for the effect of varying initial concentration. The maximum amount (q_{max}) of $REEs^{3+}$ (μg g^{-1}) adsorbed on to unmodified natural magnetite, and its corresponding concentration (mg L^{-1}) in the adsorptive carrying solution (K_L) were calculated from linear equations. The two parameters do meet, in principle, at the equilibrium adsorption point in the Langmuir curvilinear adsorption isotherm [25]. Highly and sharply curved isotherms corresponded to higher K_L and small $q_{(max)}$ (less favourable adsorption, e.g. Ce, La, Y), and lowly and gently curved isotherms corresponded to lower K_L and larger $q_{(max)}$ (more favourable adsorption, e.g. Y, Lu, Tm). It was observed that higher K_L gave a good correlation between the experimental (q_{exp}) and the calculated (q_{max}) values of adsorbate on the mineral adsorbent. The separation factor (R_L < 1) indicated that adsorption was favourable for all REEs. The correlation coefficient (R^2 = 0.97) was good and indicated that experimental data fitted strongly in the Langmuir adsorption model. Additionally, experimental data fitted well in the curvilinear expression of the Langmuir isotherm. Calculated and experimental values are presented in Table 4.

Freundlich isotherm

Experimental data from the effect of varying initial concentration was, once again, employed to plot the natural logarithm of the amount of REEs (μg g^{-1}) on the solid phase at equilibrium ($\ln q_{eql}$) as a function of the natural logarithm of $REEs^{3+}$ concentration (mg L^{-1}) in the liquid phase at equilibrium ($\ln C_{eq}$). Plot lines were obtained, from which the Freundlich isotherm constant (K_F = slope) and the adsorption intensity (n = intercept) were calculated. The values for n and K_F ((mg g^{-1})/(mg $L^{-1})^{1/n}$) are presented in Table 4 below.

The affinity of unmodified natural magnetite for $REEs^{3+}$ species, expressed as K_F (Lu (0.104), Ce (0.049) and Dy (0.071), indicated lower intensity. The adsorption intensity was greater than 1 (n > 1 or 1/n < 1) implying stronger interactions between adsorbate and adsorbent at their interface, and favourable adsorption for all $REEs^{3+}$ except Ce (n = 0.889 < 1) [22]. Plotted experimental parameters produced a good linear correlation (R^2 = 0.95), an indication that the Freundlich equation was also applicable to $REEs^{3+}$ adsorption on to unmodified natural magnetite let alone for it K_F values.

Dubinin-Radushkevich isotherm

The same experimental data from the effect of varying initial concentration was, this time around, employed to plot the natural logarithm of the amount of REEs (μg g^{-1}) on the solid phase at equilibrium ($\ln q_{eql}$) as a function of the Polanyi constant. Calculations of the later required $REEs^{3+}$ concentrations in the liquid phase (mg L^{-1}) at equilibrium (C_{eq}) [23,25]. The Dubinin-Radushkevich (D-R) isotherm

Table 2: Experimental and calculated parameters from PSO kinetic model

Kinetics	Parameter (unit)	Ce	Dy	Eu	Gd	La	Nd	Pr	Y
PSO	$q_{e\text{-}cal}$ (g mg^{-1})	0.088	0.096	0.096	0.092	0.078	0.089	0.089	0.086
	k_2 (mg g^{-1} min^{-1})	2.174	2.960	3.513	3.887	1.994	2.754	2.896	2.474
	R^2	0.9994	1.0000	0.9999	0.9998	0.9991	0.9998	0.9997	0.9993
	$q_{e\text{-}exp}$ (g mg^{-1})	0.092	0.117	0.125	0.113	0.066	0.101	0.110	0.093

Table 3: Activation energy relative to PSO kinetic model

	Ce	Dy	Eu	Gd	La	Nd	Pr	Y
K_2 / 273K	2.17	2.96	3.51	3.67	1.99	2.75	2.96	2.47
k_2 / 298K	0.66	2.18	2.20	1.58	0.71	1.46	1.46	1.05
Ea (kJ mol^{-1})	91.53	23.29	35.73	64.43	79.20	48.40	53.90	65.69

Table 4: Experimental and calculated parameters from equilibrium isotherms

Isotherm	Parameter (unit)	Ce	Dy	Eu	Gd	La	Nd	Pr	Y
Langmuir	q_{max} (mg g^{-1})	0.098	0.178	0.151	0.150	0.068	0.121	0.127	0.099
	K_L (L mol^{-1})	4.245	0.972	1.437	1.221	33.00	2.084	2.078	3.965
	R_L	0.178	0.490	0.398	0.435	0.026	0.318	0.314	0.187
	R^2	0.955	0.945	0.912	0.948	0.873	0.966	0.949	0.939
	q_{exp} (mg g^{-1})	0.092	0.117	0.125	0.113	0.066	0.101	0.110	0.093
Frendlich	K_F (mg g^{-1}) / (mol $L^{-1})^{1/n}$	0.048	0.071	0.024	0.064	0.049	0.057	0.060	0.060
	n	0.889	1.222	1.038	1.130	1.469	1.033	1.050	1.420
	R^2	0.874	0.957	0.934	0.944	0.804	0.910	0.953	0.892
	qexp (mg g^{-1})	0.092	0.117	0.125	0.113	0.066	0.101	0.110	0.093
Dubinin-Radushkevich	Xm	0.088	0.105	0.104	0.098	0.070	0.093	0.097	0.086
	K_{D-R}	2.00E-09	3.00E-09	3.00E-09	3.00E-09	2.00E-09	3.00E-09	3.00E-09	2.00E-09
	Es	1.58E+04	1.29E+04	1.29E+04	1.29E+04	1.58E+04	1.29E+04	1.29E+04	1.58E+04
	R2	0.989	0.940	0.956	0.952	0.972	0.978	0.970	0.973
	qexp	0.092	0.117	0.125	0.113	0.066	0.101	0.110	0.093

X_m and q_e (mg g^{-1}). K_{D-R} (mol^2 (kJ^2)$^{-1}$) and E_s (J mol^{-1})

Table 5: Energy parameters from thermodynamic studies

	Ce	Dy	Eu	Gd	La	Nd	Pr	Sm
K_{d1} / 298.15K	4.85	9.34	11.78	8.49	2.72	7.70	6.89	4.66
K_{d2} / 308.15K	37.24	28.93	28.87	19.61	6.74	19.67	31.81	12.95
ΔS° (J mol^{-1})	162.31	101.35	86.14	79.05	74.80	85.64	128.05	87.59
ΔH° (kJ mol^{-1})	40.75	22.61	17.93	16.73	18.16	18.76	30.60	20.43
$\Delta G°_1$ (kJ mol^{-1})	-3.59	-5.07	-5.60	-4.86	-2.27	-4.64	-4.38	-3.50
$\Delta G°_2$ (kJ mol^{-1})	-9.27	-8.62	-8.62	-7.62	-4.89	-7.63	-8.86	-6.56

constant (K_{D-R}, mol^2 (kJ mol)$^{-1}$) and the D-R adsorption capacity (X_m, mg g^{-1}) were calculated from Plot line equations. The adsorption energy, Es (J mol^{-1}), was also calculated using K_{D-R}. Table 4 below presents all calculated results. The calculated adsorption capacity (X_m), was much similar to the experimental adsorption capacity (q_e), and the correlation coefficient (R^2), indicating the fitting of experimental data in the D-R isotherm model, was consistently higher (~0.95). The energy of adsorption pointed out that the process of $REEs^{3+}$ adsorption onto unmodified natural magnetite followed an ion exchange mechanism because its values fell within the limits set in literature for this mechanism, i.e. between 8 and 16 kJ mol^{-1} [23,26].

Thermodynamic studies

Heats of adsorption

A step by step approach was employed to determine thermodynamic parameters of interest: (1) K_d were obtained from line equations of plots ($\ln(q_e/c_e)$ vs q_e) at two different temperatures (298.15K and 308.15K), (2) K_d were used in the classical Van't Hoff equation to determine Gibbs free energy, and (3) the Gibbs–Helmotz equation plots (ΔG° vs T) produced lines, the equations of which were used to calculate the standard entropy change ΔS° (slope) and the standard enthalpy change ΔH° (intercept). The distribution constant (k_d) values together with values of calculated energy changes are given in Table 5.

$$\Delta G° = -RT \ln K_{eq} \qquad \text{classical Van't Hoff equation} \qquad \text{Equation 5}$$

where R is the ideal gas constant (8.3145 J (mol^{-1} K^{-1}), T is the absolute temperature (K) and ΔG° is the standard free energy change (kJ mol^{-1}).

$$\Delta G° = \Delta H° + T\Delta S° \qquad \text{Gibbs-Helmotz equation} \qquad \text{Equation 6}$$

where ΔH° is the standard enthalpy change (kJ mol^{-1}) and ΔS° is the standard entropy change (kJ mol^{-1}).

The distribution coefficient increased with increase in temperature thereby indicating that the affinity of $REEs^{3+}$ for unmodified natural magnetite was in direct proportion relationship with temperature (Table 5). Standard free energy changes were all negative at both temperatures and, as such, indicated the feasibility and spontaneity of the adsorption of $REEs^{3+}$ onto unmodified natural magnetite at these two temperatures. In fact, ΔG° decreased with increase in temperature, making the reaction more favourable at higher temperature by increasing the mobility of adsorptive in solution and allowing more contacts between adsorptive and adsorbent. Positive standard entropy changes reflected the willingness of magnetite to take up $REEs^{3+}$ and, by so doing, compromise some surficial structural changes in order to accommodate these ions. By ΔH° and ΔS° being both positive, the spontaneity of the adsorption process ($\Delta G° < 0$) was more dependent on ΔH° than ΔS°, i.e. the difference between the energy expended in 'bond braking' ($\Delta H° > 0$) and the energy released in 'bond making' ($\Delta H° < 0$) at the activated complex could be decisive in making adsorption spontaneous ($\Delta H° < T\Delta S°$) or non-spontaneous ($\Delta H° > T\Delta S°$).

The magnitude of ΔH° gave a hint about the type of mechanism that was likely followed by $REEs^{3+}$ adsorption onto unmodified natural magnetite. Since there was no adsorption process with ΔH° between 80 – 200 kJ mol^{-1}, chemisorption was out of the possible mechanisms. Most adsorption processes had ΔH° within or slightly above the physisorption bracket of 2.1 – 20.9 kJ mol^{-1} [20]. For most REEs the mechanism predicted on the basis of E_a coincided with the one based on ΔH°.

CONCLUSION

Unmodified natural magnetite was characterised as containing Fe_3O_4 as its "sole" mineral phase by XRD. Analysis by XRF revealed that this iron oxide mineral accounted for 88.05% abundance. ICP-OES

analysis showed undetectable levels of $REEs^{3+}$ in HNO_3 leachates of unmodified natural magnetite.

Factors influencing the uptake of $REEs^{3+}$ on to unmodified natural magnetite were optimum at the following adsorption capacities: adsorbent dosage (150 mg, X μg g^{-1}), pH condition (pH = 4.5, X μg g^{-1}), agitation time (90 min, X μg g^{-1}) and initial concentration (Y mg L^{-1}, X μg g^{-1}). Trends were similar for all $REEs^{3+}$ let alone for the degree of response to influencing factors. The effect of competing ions on $REEs^{3+}$ recovery percentage was very minimal. Selectivity was higher for $REEs^{3+}$, Cu^{2+} and, moderate for Pb^{2+} and Zn^{2+}, and much lower for the rest of trace element ions in solution.

Adsorption experiments fitted the PSO kinetic model with Ea giving a split verdict, i.e. indicating a physisorption mechanism for some $REEs^{3+}$ and a chemisorption mechanism for others. Equilibrium experiments showed that the Langmuir isotherm (R^2 close to 1, q_{max} similar to q_{exp}) could explain better the adsorption processes of $REEs^{3+}$ on to unmodified natural magnetite. Thermodynamic studies indicated that adsorption processes were spontaneous ($\Delta G^o < 0$), exothermic ($\Delta H^o > 0$) and dissipative ($\Delta S^o > 0$). From the standpoint of ΔH^o (X kJ mol^{-1}) and Es (Y kJ mol^{-1}), the adsorption process was unequivocally ion exchange in nature.

ACKNOWLEDGMENT

The authors would like to express their heart felt gratitude to National Research Fund (NRF) project no. 94164 reference no. ZAM14072780687 and National Scientific and Technology counsel for funding the project (NSTC). The authors would also like to thank the support of Witwatersrand University and the University of Zambia. For the permission to access the mine area and the escort provided during the sampling exercise, the authors would like to convey their sincere thanks to the Environmental Department at Palabora Mining Company Limited (PMC Ltd) of South Africa. This work is also dedicated to the late Dr Meki Chirwa from University of Zambia, Geology Department, School of Mines, PO Box 32379, Lusaka, Zambia who suddenly passed on during the project and was part of the team. May his soul rest in peace.

ORCID IDS

Hlanganani Tutu: https://orcid.org/0000-0003-1248-130X
Luke Chimuka: https://orcid.org/0000-0002-8552-2478

REFERENCES

1. Anastopoulos I, Bhatnagar A, Lima EC. Adsorption of rare earth metals : A review of recent literature. J Mol Liq. 2016;221:954–962. doi:10.1016/j.molliq.2016.06.076.
2. Chen Z. Global rare earth resources and scenarios of future rare earth industry. J Rare Earths. 2011;29(1):1–6. doi:10.1016/S1002-0721(10)60401-2.
3. Soltani F, Abdollahy M, Petersen J, Ram R, Javad Koleini SM, Moradkhani D. Leaching and recovery of phosphate and rare earth elements from an iron-rich fluorapatite concentrate: Part II: Selective leaching of calcium and phosphate and acid baking of the residue. Hydrometallurgy. 2019;184:29–38. doi:10.1016/j.hydromet.2018.12.024.
4. Owens CL, Nash GR, Hadler K, Fitzpatrick RS, Anderson CG, Wall F. Apatite enrichment by rare earth elements : A review of the effects of surface properties. Adv Colloid Interface Sci. 2019;265:14–28. doi:10.1016/j.cis.2019.01.004.
5. Dutta T, Kim K, Uchimiya M, Kwon EE, Jeon B, Deep A, Yun S. Global demand for rare earth resources and strategies for green mining. Environ Res. 2016;150:182–190. doi:10.1016/j.envres.2016.05.052.
6. Broom-Fendley S, Brady AE, Wall F, Gunn G, Dawes W. REE minerals at the Songwe Hill carbonatite, Malawi : HREE-enrichment in late-stage apatite. Ore Geol Rev. 2017;81:23–41. doi:10.1016/j.oregeorev.2016.10.019.
7. Elsaidi SK, Sinnwell MA, Devaraj A, Droubay TC, Nie Z, Murugesan V, Mcgrail BP, Thallapally PK. Extraction of rare earth elements using magnetite@MOF composites. J Mater Chem A Mater Energy Sustain. 2018;6(38):18438–18443. doi:10.1039/C8TA04750B.
8. Wang L, Long Z, Huang X, Yu Y, Cui D, Zhang G. Recovery of rare earths from wet-process phosphoric acid. Hydrometallurgy. 2010;101(1-2):41–47. doi:10.1016/j.hydromet.2009.11.017.
9. Gergoric M, Ravaux C, Steenari B, Espegren F, Retegan T. Leaching and recovery of rare-earth elements from neodymium magnet waste using organic acids. Metals (Basel). 2018;8(9):721. doi:10.3390/met8090721.
10. Xu C, Wang L, Song W, Wu M. Carbonatites in China : A review for genesis and mineralization. Geoscience Frontiers. 2010;1(1):105–114. doi:10.1016/j.gsf.2010.09.001.
11. Negrea A, Gabor A, Davidescu CM, Ciopec M, Negrea P, Duteanu N, Barbulescu A. Rare earth elements removal from water using natural polymers. Sci Rep. 2018;8:361. doi:10.1038/s41598-017-18623-0.
12. Yang X, Makkonen HT, Pakkanen L. Rare earth occurrences in streams of processing a phosphate ore. Minerals (Basel). 2019;9(5):262. doi:10.3390/min9050262.
13. Khawassek YM, Eliwa AA, Gawad EA, Abdo SM. Recovery of rare earth elements from El-Sela effluent solutions. J. Radiat. Res. Appl. Sci. 2015;8(4):583–589. doi:10.1016/j.jrras.2015.07.002.
14. Mosai AK, Chimuka L, Cukrowska EM, Kotze' IA, Tutu H. The recovery of rare earth elements (REEs) from aqueous solutions using natural zeolite and bentonite. Water Air Soil Pollut. 2019;230(8):188. doi:10.1007/s11270-019-4236-4.
15. Ogata T, Narita H, Tanaka M, Hoshino M, Kon Y, Watanabe Y. Selective recovery of heavy rare earth elements from apatite with an adsorbent bearing immobilized tridentate amido ligands. Separ Purif Tech. 2016;159:157–160. doi:10.1016/j.seppur.2016.01.008.
16. Koduru JR, Lingamdinne LP, Kailasa SK, Thenepalli T, Chang YY, Yang JK. Recent strategies on adsorptive removal of precious metals and rare earths elements using low-cost natural adsorbent. In: Jyothi R, editor. *Rare-earth metal recovery for green technologies*. Springer, Cham; 2020. p. 87–109. doi:10.1007/978-3-030-38106-6_5.
17. Granados-Correa F, Vilchis-Granados J, Jiménez-Reyes M, Quiroz-Granados LA. adsorption behaviour of La (III) and Eu (III) ions from aqueous solutions by hydroxyapatite: kinetic, isotherm, and thermodynamic studies. J Chem. 2013;2013(1):751696. doi:10.1155/2013/751696.
18. Ugwu IM, Igbokwe OA. Advanced sorption process applications. Sorption of heavy metals on clay minerals and oxides: A Review. In: Edebali S (editor), Advanced Sorption Process Applications. IntechOpen; 2019. p. 23. doi:10.5772/intechopen.80989.
19. Alorro RD, Hiroyoshi N, Kijitani H, Ito M, Tsunekawa M. On the use of magnetite for gold recovery from chloride solution. Miner Process Extr Metall Rev. 2010;31(4):201–213. doi:10.1080/08827508.2010.483359.
20. Saha P, Chowdhury S. Insight into adsorption thermodynamics. Tadashi M (editor), Thermodyanamics. IntechOpen; 2011. p. 349–364. doi:10.5772/13474.
21. Kajjumba GW, Emik S, Öngen A, Özcan HK, Aydın S. Advanced sorption process applications. Modelling of adsorption kinetic processes — Errors, theory and application. In: Edebali S (editor), Advanced Sorption Process Applications. IntechOpen; 2018. p. 19.
22. Lyubchik S, Lyubchik A, Lygina O, Lyubchik S, Fonseca I. Comparison of the thermodynamic parameters estimation for the adsorption process of the metals from liquid phase on activated carbons. In: Moreno-Pirajan JC (editor), Thermodyanamics – Interaction Studies – Solids, Liquids and Gases. IntechOpen; 2011. p. 95–122. doi:10.5772/19514.
23. Mihaly-Cozmuta L, Mihaly-Cozmuta A, Peter A, Nicula C, Tutu H, Silipas D, Indrea E. Adsorption of heavy metal cations by Na-clinoptilolite : equilibrium and selectivity studies. J Environ Manage. 2014;137:69–80. doi:10.1016/j.jenvman.2014.02.007.
24. Santos Yabe MJ, de Oliveira E. Heavy metals removal in industrial effluents by sequential adsorbent treatment. Adv Environ Res. 2003;7(2):263–272. doi:10.1016/S1093-0191(01)00128-9.
25. Bleam WF. Chapter 8 - Surface Chemistry and adsorption. In: Soil and environmental chemistry, 2nd edition. Academic Press; 2017. pp. 385–443. doi:10.1016/B978-0-12-804178-9.00008-2.
26. Inglezakis VJ, Zorpas AA. Heat of adsorption, adsorption energy and activation energy in adsorption and ion exchange systems. Desalin. Water Treat. 2012;39(1-3):149–157. doi:10.5004/dwt.2012.3000.